Cerebral Cortex August 2009;19:1820–1834
doi:10.1093/cercor/bhn212
Advance Access publication November 19, 2008

Dopamine D_1 and D_5 Receptors Are Localized to Discrete Populations of Interneurons in Primate Prefrontal Cortex

Jill R. Glausier[1,2], Zafar U. Khan[3] and E. Chris Muly[1,2,4]

[1]Division of Neuroscience, Yerkes National Primate Research Center, Atlanta, GA 30329, USA, [2]Department of Psychiatry and Behavioral Sciences, Emory University, Atlanta, GA 30322, USA, [3]Laboratory of Neurobiology, Centro de Investigaciones Medico-Sanitarias (CIMES), Faculty of Medicine, University of Malaga, Malaga, Spain and [4]Department of Veterans Affairs Medical Center, Decatur, Atlanta, GA 30033, USA

Working memory (WM) is a core cognitive process that depends upon activation of D1 family receptors (D1R) and inhibitory interneurons in the prefrontal cortex (PFC). D1R are comprised of the D_1 and D_5 subtypes, and D_5 has a 10-fold higher affinity for dopamine. Parvalbumin (PV) and calretinin (CR) are 2 interneuron populations that are differentially affected by D1R stimulation and have discrete postsynaptic targets, such that PV interneurons provide strong inhibition to pyramidal cells, whereas CR interneurons inhibit other interneurons. The distinct properties of both the D1R and interneuron subtypes may contribute to the "inverted-U" relationship of D1R stimulation and WM ability. To determine the prevalence of D_1 and D_5 in PV and CR interneurons, we performed quantitative double-label immunoelectron microscopy in layer III of macaque area 9. We found that D_1 was the predominant D1R subtype in PV interneurons and was found mainly in dendrites. In contrast, D_5 was the predominant D1R subtype in CR interneurons and was found mainly in dendrites. Integrating these findings with previously published electrophysiological data, we propose a circuitry model as a framework for understanding the inverted-U relationship between dopamine stimulation of D1R and WM performance.

Keywords: calretinin, electron microscopy, parvalbumin, synapses, working memory

Introduction

Dopamine activation of D1 family receptors (D1R) in the prefrontal cortex (PFC) regulates PFC functions, especially working memory (WM) (Brozoski et al. 1979; Sawaguchi and Goldman-Rakic 1991; Muller et al. 1998). There is an inverted-U relationship between D1R activation and WM performance, such that both too much or too little D1R activation results in diminished WM performance (reviewed in Goldman-Rakic et al. 2000). The cellular basis of WM is pyramidal cells that respond to discrete cues selectively during the delay period of WM tasks. Both the activity and the accuracy, or tuning, of these "delay cells" are modulated by D1R activation in a dose-dependent manner (Williams and Goldman-Rakic 1995; Vijayraghavan et al. 2007). Tuned delay activity has also been identified in putative inhibitory interneurons of the PFC (Wilson et al. 1994; Rao et al. 1999), and blockade of GABAergic neurotransmission abolishes tuned neuronal responses (Rao et al. 2000) and impairs WM performance (Sawaguchi et al. 1988, 1989; Sawaguchi and Iba 2001). Given the importance of GABAergic and D1R activity for PFC functioning, it is important to determine how these 2 relate within prefrontal circuitry.

Cortical interneurons can be subdivided by the presence of calcium-binding proteins such as parvalbumin (PV) and calretinin (CR) (Conde et al. 1994; Gonchar and Burkhalter 1997; Kawaguchi and Kubota 1997). PV interneurons are chandelier and basket cells and are the strongest source of inhibition to pyramidal cells (Williams et al. 1992; Gonzalez-Burgos, Krimer, et al. 2005). CR interneurons comprise approximately 50% of the total interneuron population in monkey PFC (Conde et al. 1994). They typically exhibit double bouquet morphology and primarily synapse onto dendrites, the majority of which belong to GABAergic interneurons (Gabbott and Bacon 1996; Meskenaite 1997; Melchitzky and Lewis 2008). Thus, activation of CR neurons may result in the disinhibition of a pyramidal cell (Wang et al. 2004). The disparate effects PV and CR interneurons can have on pyramidal cell output identify them as key circuit components that might mediate the inverted-U relationship between D1R activation and WM function.

The D1R are comprised of the D_1 and D_5 subtypes (Grandy et al. 1991; Sunahara et al. 1991; Tiberi et al. 1991), and their activation typically enhances the excitability of pyramidal cells and interneurons (reviewed in Seamans and Yang 2004). Intriguingly, the D_5 receptor has a 10-fold higher affinity for dopamine than the D_1 receptor (Sunahara et al. 1991; Weinshank et al. 1991). Although they cannot be distinguished by currently available pharmacological tools, subtype-specific antibodies are available, and we have recently shown that D_1 and D_5 are colocalized in pyramidal cell spines and axon terminals in PFC (Bordelon-Glausier et al. 2008). However, the prevalence and subcellular localization of a given receptor can differ between pyramidal cells and interneuron subtypes (Disney et al. 2006). A previous immunofluorescence study has found evidence for differential prevalence of the D_1 receptor in the cell bodies of interneuron subtypes (Muly et al. 1998); however, this study did not quantify the extent to which D_1 was found in the dendritic and axonal arbors of different interneuron populations nor was the distribution of the other D1R subtype, D_5, examined. The present study was undertaken to specifically examine these questions. We hypothesized that, like pyramidal cell spines (Bordelon-Glausier et al. 2008), D_5 would be colocalized with D_1, and both D1R would be primarily localized to PV interneuron dendrites. To the contrary, our results demonstrate that D_1 and D_5 dopamine receptors are differentially localized to PV and CR dendrites and axon terminals. PV interneurons contain abundant D_1 (17.3% of dendritic profiles) but significantly less D_5 (4.7% of dendritic profiles), and CR interneurons contain abundant D_5 (15% of dendritic profiles) but significantly less D_1 (4% of dendritic profiles).

Materials and Methods

Animals and Preparation of Tissue

Tissue from 7 *Macaca mulatta* monkeys was used for this study. The care of the animals and all anesthesia and sacrifice procedures in this

study were performed according to the National Institutes for Health Guide for the Care and Use of Laboratory Animals and were approved by the Institutional Animal Care and Use Committee of Emory University. The animals were sacrificed with an overdose of pentobarbital (100 mg/kg) and then perfused with a flush of Tyrode's solution. The flush was followed by 3–4 L of fixative solution of 4% paraformaldehyde/0.1–0.2% glutaraldehyde/0–0.2% picric acid in phosphate buffer (0.1 M, pH 7.4). The brain was blocked and postfixed in 4% paraformaldehyde for 2–24 h. Coronal, 50-μm thick vibratome sections of prefrontal cortical area 9 (Walker 1940), were cut and stored frozen at –80 °C in 15% sucrose until immunohistochemical experiments were performed.

Antisera

Four antibodies were used in this study: mouse anti-PV (Sigma-Aldrich, St Louis, MO), mouse anti-CR (Swant, Switzerland), rat anti-D_1 (Sigma-Aldrich), and rabbit anti-D_5 (Khan et al. 2000). The mouse anti-PV antibody recognizes a single band at a molecular weight of approximately 12 kDa in western blot analysis (Celio 1986; Park et al. 2008) and does not cross react with GABA, glutamate (Celio 1986), or other members of the EF-hand family (Sigma-Aldrich Product Information); and histochemical labeling is abolished when the antisera are preabsorbed with purified muscle PV (Heizmann and Celio 1987). The mouse anti-CR antibody recognizes a single band at a molecular weight of approximately 29 kDa in western blot analysis and does not cross react with the highly related protein calbindin-D28k (Zimmermann and Schwaller 2002). The characterization of the rat anti-D_1 and rabbit anti-D_5 antisera has been previously described in detail (Bordelon-Glausier et al. 2008). Briefly, the rat anti-D_1 antibody stains one major band in western blot analysis of rat brain membranes at 65–75 kDa (Hersch et al. 1995), and all staining at the light and electron microscopic levels was abolished when the antiserum was preincubated with a D_1–glutathione-S-transferase (GST) fusion protein (Smiley et al. 1994). The rabbit anti-D_5 antibody does not react with Sf9 cells expressing any other dopamine receptor (Khan et al. 2000), labels a single band at approximately 53–54 kDa, and immunohistochemical staining was abolished when the antibody was preincubated with the cognate peptide (Bordelon-Glausier et al. 2008). Both the D_1 and D_5 antibodies penetrate through the depth of a 50-μm tissue section (data not shown), when examined as previously described (Muly et al. 2001).

Double-Label Immunohistochemistry

To examine the presence of D_1 and D_5 in cortical interneurons, double-label experiments were performed. A preembedding immunogold/diaminobenzidine (DAB) protocol was used in which immunogold was used to label PV or CR and D_1 or D_5 was labeled with DAB. Tissue sections were thawed and incubated with blocking serum (3% normal goat serum, 1% bovine serum albumin, 0.1% glycine and lysine, and 0.5% fish gelatin made in phosphate-buffered saline) for 1 h at room temperature. Sections were incubated overnight in a cocktail of primary immunoreagents (rat anti-D_1, 1:500 or rabbit anti-D_5, 1:500; and mouse anti-PV, 1:10 000 or mouse anti-CR, 1:10,000), followed by an overnight incubation in a cocktail of secondary antisera (biotinylated donkey anti-rat at 1:200, Jackson ImmunoResearch, West Grove, PA; or biotinylated goat anti-rabbit at 1:200, Vector, Burlingame, CA; and 1-nm gold-conjugated goat anti-mouse at 1:200, Nanoprobes, Yaphank, NY). Sections were then postfixed in 2% glutaraldehyde for 20 min and silver intensified for 3–5 min using the HQ Silver kit (Nanoprobes). An incubation in ABC reagent for 1 h at room temperature followed (Vector, Burlingame, CA), and sections were then reacted with DAB and 0.3%H_2O_2. Tissue sections were then osmicated in 0.5% OsO_4 for 10 min, dehydrated in ethanol and propylene oxide, and flat embedded in Durcupan resin. Control sections, in which 1 of the 2 primary immunoreagents was omitted, showed no evidence either for nonspecific deposition of gold particles (except for cell nuclei, which we find nonspecifically interact with gold-labeled antibodies) or for nonspecific deposition of DAB onto previously developed gold particles. Furthermore, each antibody only produced labeling when incubated the corresponding secondary antibody, demonstrating that spurious immunolabeling is unlikely in the double-labeled conditions (Fig. 1).

Analysis of Material

At least 2 blocks from each of the 3–4 animals in each type of double-label experiment were examined. The blocks were made from layer III of cortical area 9; 60-nm ultrathin sections were cut and examined using a Zeiss EM10C electron microscope. Layer III was chosen

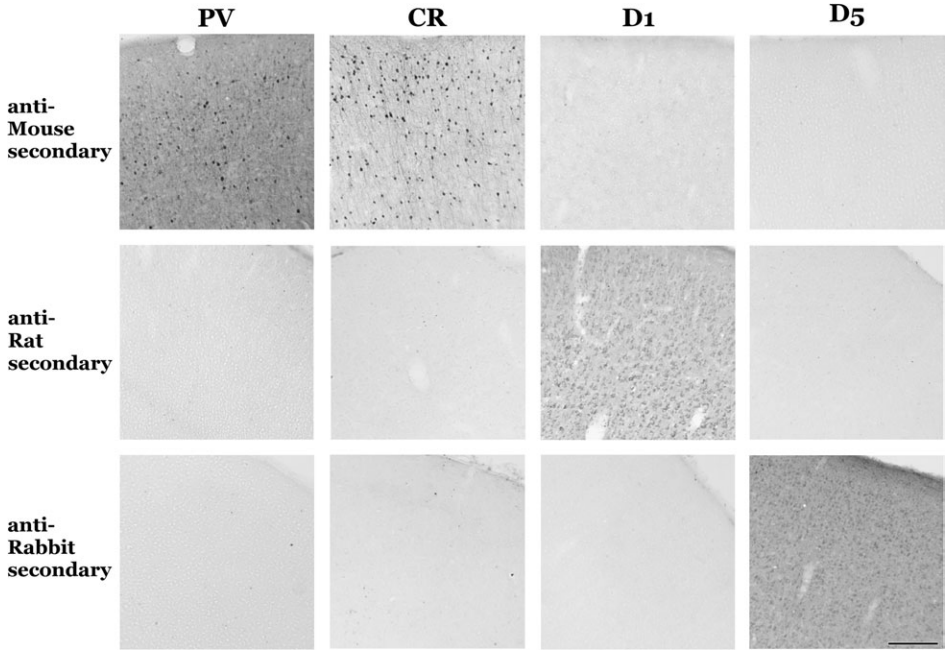

Figure 1. Light microscopic images demonstrating that each antibody used in this study only produced labeling when incubated with the appropriate secondary antibody. The mouse anti-PV and mouse anti-CR antibodies only produce labeling when incubated with an anti-mouse secondary. The rat anti-D_1 antibody only produced labeling when incubated with anti-rat secondary, and the rabbit anti-D_5 antibody only produced labeling when incubated with anti-rabbit secondary. Scale bar is 500 μm.

because it is a major site of cortical integration (Rockland and Pandya 1979; Maunsell and van Essen 1983; Kritzer and Goldman-Rakic 1995), and both receptors are concentrated in dendritic structures in this layer (Bordelon-Glausier et al. 2008). Regions of the grids containing neuropil were selected for analysis-based ultrastructural preservation and adequate DAB staining among the immunogold labeling. Electron micrographs of immunogold-containing dendrites and axon terminals (immunoreactive for PV or CR) were taken, and these profiles were then examined for the presence of immunoperoxidase label (D_1 or D_5). Images were collected at a magnification of 31 500 using a Dualvision cooled CCD camera (1300 × 1030 pixels) and Digital Micrograph software (version 3.7.4, Gatan, Inc., Pleasanton, CA). For D_1/PV, a total of 423 micrographs from 4 monkeys representing 2580 μm^2 were analyzed. For D_1/CR, a total of 330 micrographs from 3 monkeys representing 2013 μm^2 were analyzed. For D_5/PV, a total of 411 micrographs from 4 monkeys representing 2507 μm^2 were analyzed. For D_5/CR, a total of 434 micrographs from 4 monkeys representing 2647 μm^2 were analyzed. The percentage of PV and CR profiles which contained label for either D_1 or D_5 was tabulated and compared with a chi-square analysis. All *p* values are reported as Fisher's exact *p* value.

Images containing PV- or CR-labeled dendrites were further analyzed to determine 1) if they were synaptically contacted by axon terminals and, if so, whether the axon terminal displayed D_1- or D_5-immunoreactivity (IR); 2) their perimeter; and 3) their diameter. Synapses were identified as asymmetric or symmetric based on ultrastructural criteria (Peters 1987). After determining the frequency of synaptic contacts onto PV- and CR-labeled dendrites, their perimeter was determined so that the density of synaptic contacts could be calculated. To determine the perimeter of PV- and CR-labeled dendrites, each image was saved in tagged imagine file format (TIFF) and imported into an image processing program (Canvas 8, Deneba Software) where the TIFF was reduced in size by 40%. The immunogold-labeled dendrites were then outlined, and a conversion factor was used to determine the perimeter in microns. A total PV perimeter length of 1,513.92 μm and a total CR perimeter length of 1,359.59 μm were examined. Density of synaptic contacts was calculated as the total number of synaptic contacts divided by the total perimeter length examined. Finally, the diameter of each PV- and CR-labeled dendrite was determined and used to indicate the proximity of a dendrite to its cell body. To determine the diameter, a straight line was drawn in cross section across the dendrite, and the same conversion factor was used to determine that length in microns. For dendrites cut in transverse section, the shortest diameter was measured. The diameter of 605 PV-labeled dendrites and 589 CR-labeled dendrites was measured.

To examine the location of the D1R within a dendrite, we analyzed single and serial sections. In the single section analysis, each DAB patch in a PV- or CR-labeled dendrite was categorized as touching the plasma membrane or intracellular. If the DAB patch was touching the plasma membrane, we also determined if it was associated with any visible synapses. Using DAB to examine the location of a receptor has been used previously (Sarro et al. 2008), and the particularly patchy nature of the D1R DAB label makes this type of analysis possible. We also examined the location of D1R DAB label using serial section electron microscopy (EM) analysis. PV- and CR-labeled dendrites were followed for 8–10 serial sections on one grid and examined for the presence and location of DAB and synaptic inputs.

Results

Localization of D^1 and D^5 in PV- and CR-Labeled Cell Bodies

Although the primary goal of this study was to determine the extent of D1R localization in the dendritic and axonal arbors of cortical interneurons, we also examined PV and CR immunogold-labeled cell bodies for the presence of D_1 and D_5 DAB label. As previously reported (Muly et al. 1998), D_1-immunoreactivity (IR) was commonly seen in PV-labeled cell bodies but rarely seen in CR-labeled somata. In the present study, we also examined D_5-IR and found the opposite pattern. D_5-IR was commonly seen in CR-labeled cell bodies but rarely in PV-labeled cell bodies. The D_1 labeling pattern within PV somata was similar to that seen in pyramidal cell somata (Smiley et al. 1994; Bordelon-Glausier et al. 2008), that is, D_1-IR was principally located on the Golgi apparatus (Fig. 2*A*), though labeling with other internal membranes (Fig. 2*B*) and the plasma membrane was also identified. D_5 labeling within CR cell bodies was also consistent with that observed in pyramidal cell somata (Bordelon-Glausier et al. 2008), being associated with a variety of internal membranes (Fig. 2*C*) and the plasma membrane.

Colocalization of D^1 or D^5 in PV Interneurons

PV-containing dendrites in PFC are nonpyramidal local circuit interneurons (Williams et al. 1992; Lund and Lewis 1993); however, PV-containing axon terminals may arise from 2 sources: PV interneurons and thalamocortical axons

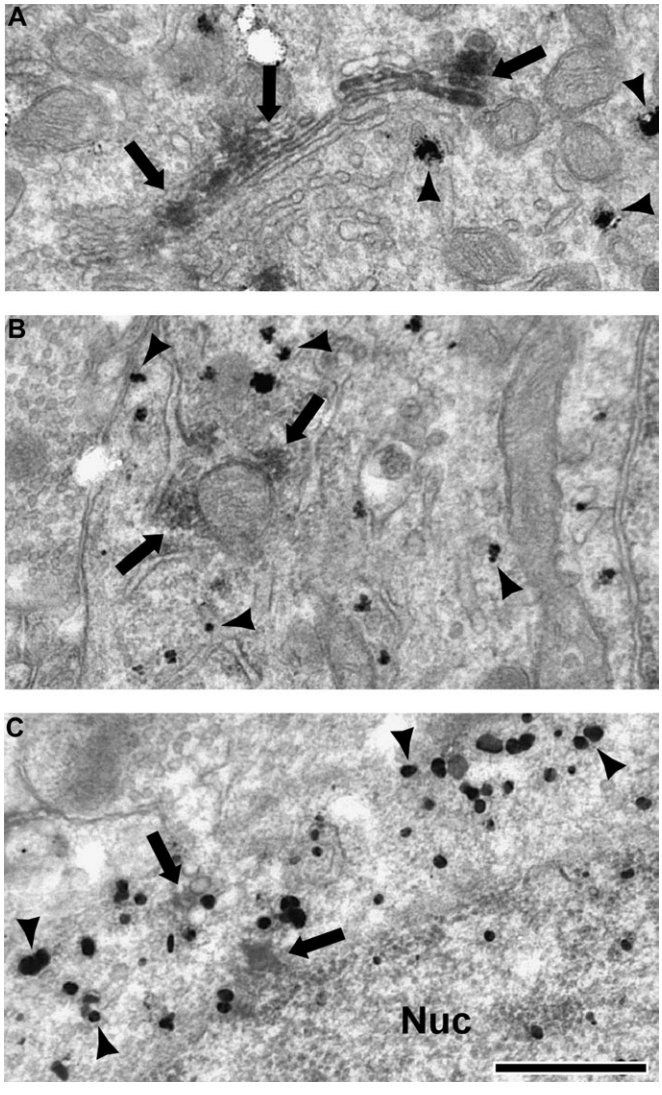

Figure 2. Electron micrographs of cell bodies immunogold labeled for PV or CR (black arrowheads) which also contain DAB label (black arrows) for D_1 and D_5. In PV somata, the stereotypical D_1 staining of the Golgi apparatus was identified (*A*), as well as labeling associated with other internal membrane structures, including endoplasmic reticulum and mitochondria (*B*). In CR somata, D_5 staining was associated with internal membranes (*C*). Nucleus (Nuc). Scale bar is 500 nm.

(Goldman-Rakic and Porrino 1985; Giguere and Goldman-Rakic 1988; Jones and Hendry 1989; Williams et al. 1992; Melchitzky et al. 1999). PV-IR thalamocortical terminals are found primarily in deep layer III and layer IV and make asymmetric synapses (Giguere and Goldman-Rakic 1988; Melchitzky et al. 1999). In our blocks, taken primarily from superficial layer III, we identified 356 PV-labeled terminals. Many of these terminals did not display synaptic specializations in the 60-nm ultrathin tissue section; thus, we could not identify what type of synapse, if any, those PV-labeled terminals were making. However, 68 of the 356 PV-labeled axon terminals did make identifiable synapses, with some terminals making more than 1 synapse. Only 4 of the 70 identified synapses were asymmetric, whereas the other 66 displayed symmetric specializations (Fig. 3*D*), indicating that our sample of PV-labeled terminals is largely from interneuron axons. Of the 66 symmetric synapses formed by PV terminals, 33 were onto dendritic spines, 28 were onto dendritic shafts, and 5 were onto a soma. These results are consistent with a previous quantitative EM study examining PV terminations in the PFC (Melchitzky et al. 1999).

Dendrites (Fig. 3*A–C*) that contained immunogold label for PV were identified and then examined for the presence of DAB label for either D_1 or D_5. The frequency of PV-labeled dendritic profiles that contain D_1 (17.3%, 53 of 307) was greater than the frequency of PV-labeled dendritic profiles that contain D_5 (4.7%, 14 of 296), and this difference was statistically significant (Fig. 4; $\chi^2 = 23.971$, $p < 0.0001$). Axon terminals (Fig. 3*D*) that contained immunogold label for PV were also identified and examined for the presence of DAB label for either D_1 or D_5. Similar to PV dendrites, the frequency of PV-labeled axon

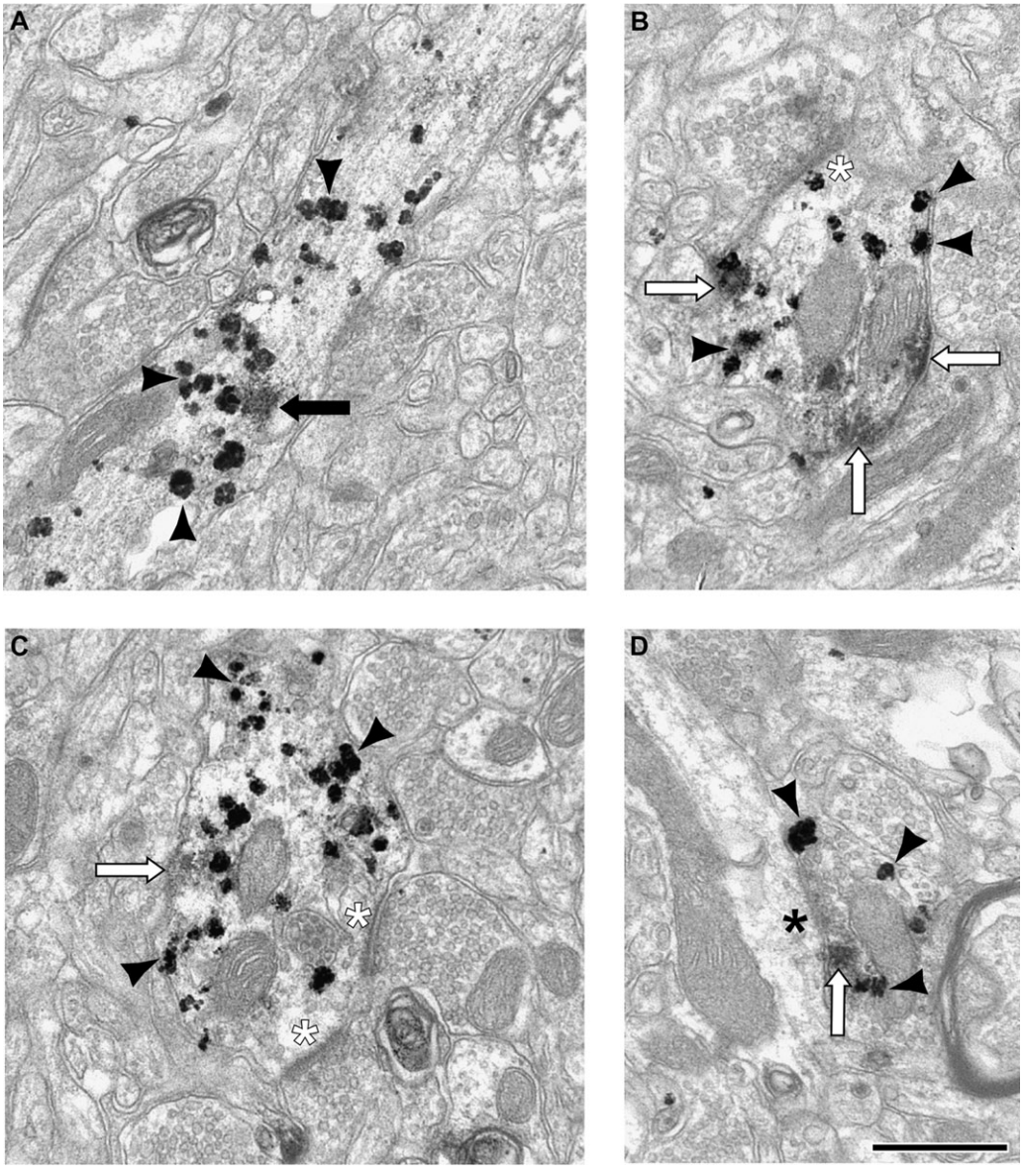

Figure 3. Electron micrographs of dendrites (*A–C*) and an axon terminal (*D*) labeled for PV with immunogold (black arrowheads) and D_1 with DAB. White arrows indicate DAB which contacts the plasma membrane (*B–D*), and black arrows indicate DAB which is intracellular (*A*). Note the D_1 DAB label is discrete and patchy. PV-labeled dendrites often received asymmetric synapses (*B*, *C*, white asterisks). PV-labeled axon terminals were typically observed to make symmetric synaptic contacts onto unlabeled dendrites (*D*, black asterisk). Scale bar is 500 nm.

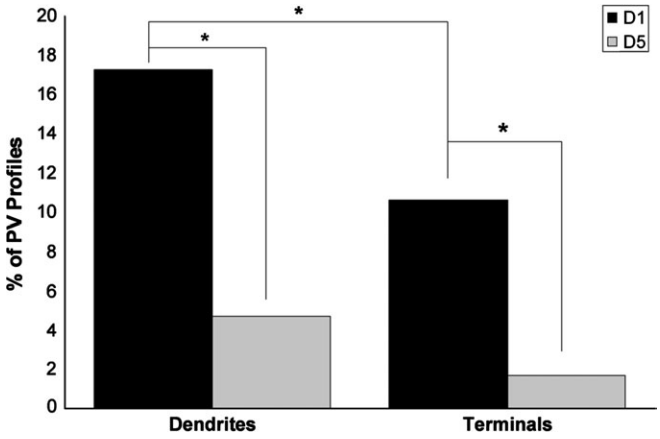

Figure 4. A histogram showing the percentage of PV-labeled dendrites and axon terminals that also contained IR for D_1 and D_5. In tissue double-labeled for D_1 and PV, 307 PV-IR dendrites and 179 axon terminals in total were counted. In tissue double labeled for D_5 and PV, 296 dendrites and 177 axon terminals in total were counted. The frequency of D_1/PV dendrites (17.3%) and axon terminals (10.6%) is greater than the frequency of D_5/PV dendrites (4.7%) and axon terminals (1.7%). D_1-IR was also more frequently identified in PV dendrites than axon terminals. Asterisks indicate a significant difference.

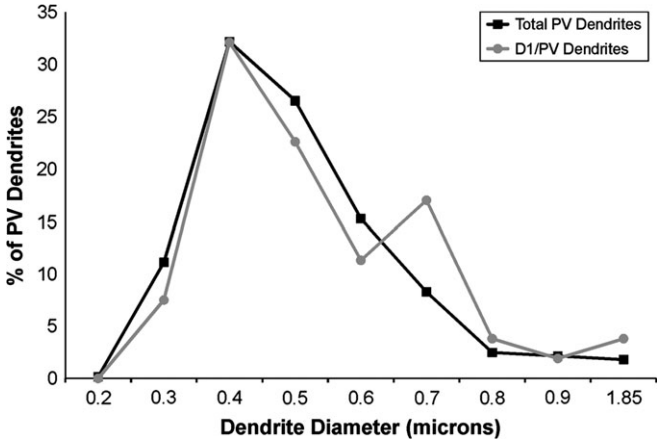

Figure 5. Graph illustrating the distribution of all PV dendritic diameters ($N = 603$) and the distribution of the diameters of D_1/PV double-labeled dendrites ($N = 53$). The majority of PV dendrites had diameters between 0.4 and 0.5 μm in diameter, as did D_1/PV double-labeled dendrites. These results indicate that D_1 labeling is not found preferentially in small (distal) or large (proximal) caliber PV dendrites.

terminal profiles that contain D_1 (10.6%, 19 of 179) was greater than the frequency of PV-labeled axon terminal profiles that contained D_5 (1.7%, 3 of 177), and this difference was also statistically significant ($\chi^2 = 12.212$, $p = 0.0006$). In material double labeled for PV and D_1, D_1 label was more prevalent in dendrites than axon terminals ($\chi^2 = 3.961$, $p = 0.0480$).

We next sought to determine if there was preferential D_1 labeling of proximal or distal PV dendrites. The diameter of all PV-labeled dendrites was calculated and used to determine its proximity to the cell body. Although the tapering of interneuron dendrites is not as pronounced as in pyramidal cells, there is a general correlation between dendrite diameter and its proximal or distal location in the dendritic arbor (Jones 1975; Peters and Jones 1984). The vast majority of PV-labeled interneurons examined had a diameter of less than 1 μm (597 of 605 PV-labeled dendrites), and the diameter of D_1/PV double-labeled dendrites mirrored the overall distribution of PV-labeled dendrites (Fig. 5). These observations indicate that there was no preferential D_1 labeling of large versus small PV dendrites.

Finally, single and serial section analysis was used to examine the localization of D_1 DAB IR within PV-labeled dendrites. Within single ultrathin sections, 34% of the D_1/PV double-labeled dendrites had D_1 DAB that was touching the plasma membrane (18 of 53 dendrites), and 3 of these 18 DAB patches were associated with an asymmetric synapse. Serial section analysis provided a more complete picture of how D_1 DAB was distributed throughout a PV-labeled dendrite (Fig. 6). In this PV-labeled dendrite, D_1-IR is associated with internal membranes (panels B–J) and the plasma membrane (panels C and D and G–J). In panel D, a tangentially cut asymmetric synapse is visible on the far right, and a patch of D_1-IR is present adjacent to the synapse. In panels E and F, an asymmetric synapse is visible at the 12 o'clock position, and plasma membrane–associated IR is present in the same location in panels G and H. Taken together, these results indicate that the D_1 receptor is the predominate type of D1R localized to PV interneurons of the primate PFC, and D_1-IR is associated with the plasma membrane and asymmetric synapses onto PV-labeled dendrites.

Colocalization of D^1 or D^5 in CR Interneurons

CR cells in the PFC are nonpyramidal local circuit interneurons that frequently display double bouquet morphology and are densest in layers I–IIIa (Conde et al. 1994). Dendrites (Fig. 7*A,B*) and axon terminals (Fig. 7*C,D*) containing immunogold label for CR were identified. We identified 203 CR-labeled axon terminals, and the synaptic specialization was identifiable in 42 of the single sections through CR-labeled axon terminals. Of these, 85.7% (36 of 42) were making symmetric synapses, and 14.3% (6 of 42) were making asymmetric synapses. Of the 36 symmetric synapses formed by CR-labeled axon terminals, 27 were onto dendritic shafts, 5 were onto spines, and 4 were onto a soma. These data indicate that the vast majority of the CR-labeled terminals sampled originate from inhibitory interneurons, which is in agreement with a previous report that 93% of CR-IR terminals in superficial cortical layers form symmetric synapses (Melchitzky et al. 2005).

We quantified the extent to which CR-labeled dendrites and terminals also contained D_1-IR or D_5-IR. In contrast to what was observed for PV-labeled dendrites, the frequency of CR-labeled dendritic profiles that contained D_5 (15.0%, 47 of 313 dendritic profiles) was greater than the frequency of CR dendritic profiles that contained D_1 (4.0%, 11 of 276 dendritic profiles). This difference was statistically significant (Fig. 8; $\chi^2 = 20.102$, $p < 0.0001$). Neither D_1-IR (1.3%, 1 of 79) nor D_5-IR (5.8%, 8 of 139) was commonly observed in CR-labeled axon terminals, and the number of observations in the D_1/CR double-label experiment was not sufficient to allow a valid statistical comparison between D_1/CR and D_5/CR axon terminal frequencies. When comparing the distribution of D_5-IR in CR-labeled profiles, the D_5 receptor is more prevalent in CR dendrites than axon terminals ($\chi^2 = 7.724$, $p = 0.0048$).

The diameter of each CR-labeled dendrite was then calculated and used as an estimate of its proximity to the cell body. The vast majority of CR-labeled interneurons examined had a diameter of less than 1 μm (576 of 589 CR-labeled dendrites), and the diameter of D_5/CR double-labeled dendrites mirrored the overall distribution of CR-labeled dendrites

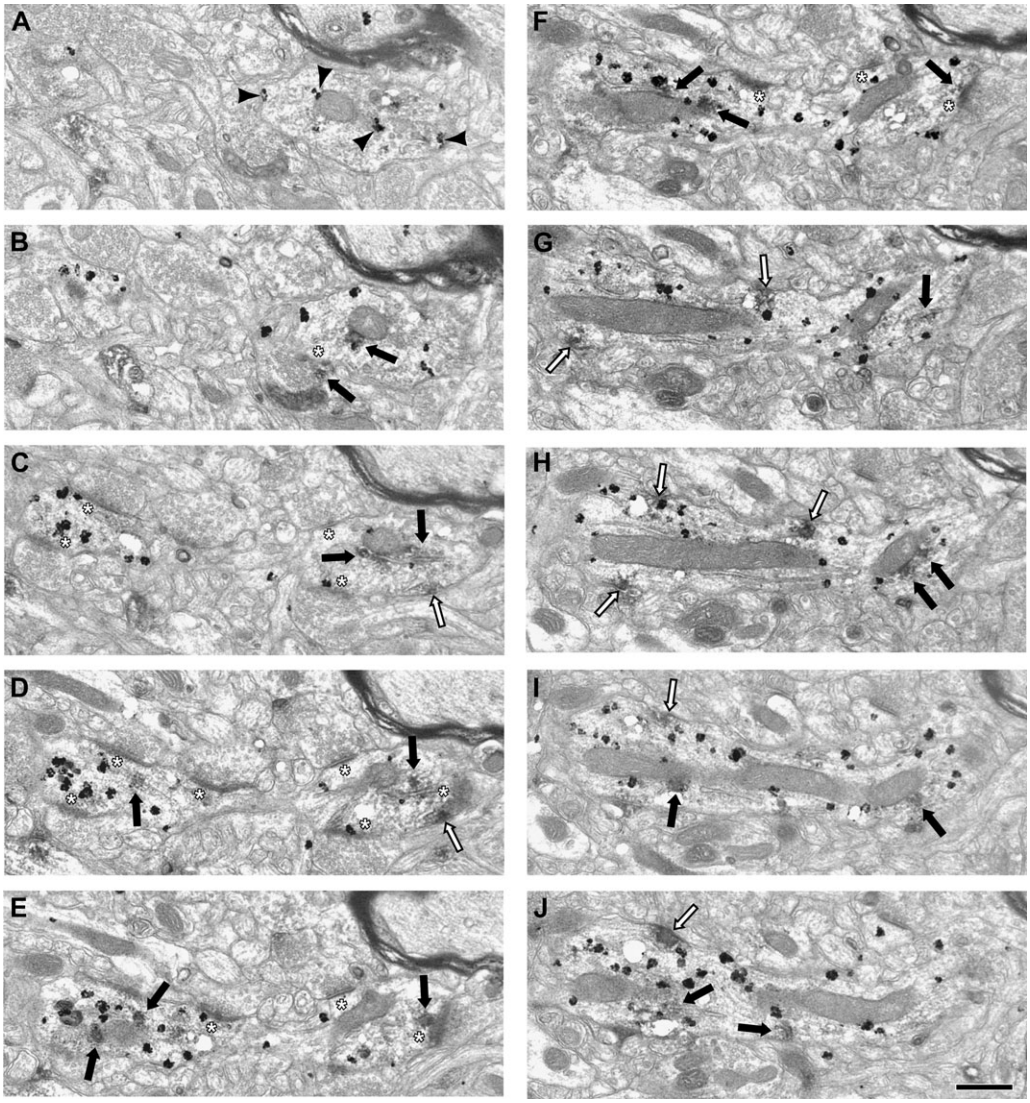

Figure 6. Electron micrographs illustrating the distribution of D_1-IR in serial sections of a PV-labeled dendrite. PV immunogold label is present throughout the dendrite and is identified by black arrowheads in panel (*A*). Patches of D_1-IR have been identified as intracellular (black arrows) or associated with the plasma membrane (white arrows). In panel (*A*), no D_1-IR appears in the PV dendrite. However, in panel (*B*), D_1-IR is present and associated with the mitochondria. The beginnings of an asymmetric synapse appear (white asterisk), and the terminal contains D_1-IR. Also, a continuation of the PV-labeled dendrite is present on the left side of the image. On the right side in panel (*C*), D_1-IR is present associated with the plasma membrane as well as internal membranes. The beginnings of another asymmetric synapse are also visible (white asterisk). On the left of panel (*C*), 2 asymmetric synapses are visible. In panel (*D*), D_1-IR is present internally and associated with internal membranes as well as the plasma membrane. In panels (*E* and *F*), the D_1-IR is located intracellularly, and one DAB patch is directly below an asymmetric synapse in both panels. In panels (*G*–*J*), D_1-IR is associated with the plasma membrane and mitochondria, and synapses are no longer visible. Scale bar is 500 nm.

(Fig. 9). These observations indicate that there was no preferential D_5 labeling of large or small CR dendrites.

Finally, single and serial section analysis was used to examine the localization of D_5 DAB IR within CR-labeled dendrites. Within single ultrathin sections, 38% of the D_5/CR double-labeled dendrites had D_5 DAB that was touching the plasma membrane (18 of 47 dendrites). However, only 3 of the 47 CR-labeled dendrites were receiving identifiable asymmetric synapses; thus, the association of D_5 DAB with asymmetric synapses could not be ascertained from single section analysis. Serial section analysis provided a more complete picture of how D_5 DAB was distributed throughout a CR-labeled dendrite (Fig. 10). In this individual CR-labeled dendrite, D_5-IR is associated with internal membranes (panels C and D) and the plasma membrane (panel A). These results indicate that D_5 is the predominant D1R localized to CR interneurons, and it is found intracellularly and associated with the plasma membrane.

Synaptic Frequency and Density onto PV and CR Dendrites

To determine the frequency of synapses onto PV- and CR-labeled dendrites, 546 sections through PV-labeled dendrites and 451 sections through CR-labeled dendrites were examined for the presence of asymmetric or symmetric contacts. Significantly, more PV-labeled dendrites received synapses than CR-labeled dendrites (46% of PV-labeled dendritic profiles vs. 38% of CR-labeled dendritic profiles, $\chi^2 = 7.166$, $p = 0.0083$). The synaptic contacts onto PV-labeled dendritic profiles were more likely to be asymmetric than those onto CR-labeled dendritic profiles (91% vs. 69%, $\chi^2 = 38.835$, $p < 0.0001$). These

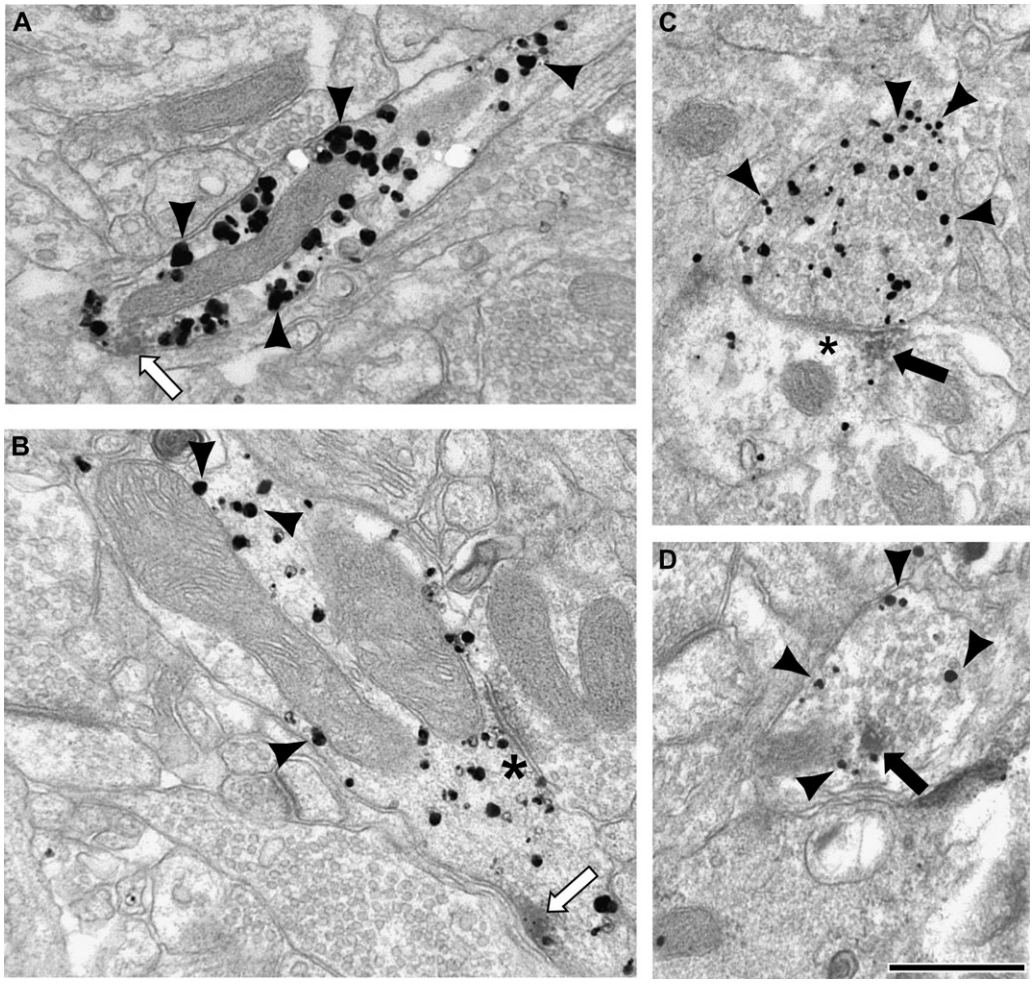

Figure 7. Electron micrographs of dendrites (*A*, *B*) labeled with immunogold (black arrowheads) for CR and DAB for D_5. White arrows indicate DAB which contacts the plasma membrane (*A*, *B*), and black arrows indicate DAB which is intracellular (*C*, *D*). Note the D_5 DAB label is discrete and patchy. (*B*) The D_5/CR-labeled dendrite is receiving a symmetric synapse (black asterisk) from an unlabeled terminal. (*C*) CR immunogold-labeled axon terminal making a symmetric synapse (black asterisk) onto a single-labeled dendrite containing D_5 DAB intracellularly. (*D*) CR immunogold-labeled axon terminal also containing intracellular D_5 DAB label. Scale bar is 500 nm.

results are consistent with a previous report examining local axon termination onto PV and CR interneurons which found that PV dendrites receive a higher frequency of excitatory inputs than CR dendrites (Melchitzky and Lewis 2003).

Next, the perimeter of each PV- and CR-labeled dendrite was calculated so that the density of asymmetric and symmetric synapses onto PV- and CR-labeled dendrites could be determined. The average perimeter of a section through a PV-labeled dendrite was 2.76 μm, and the average perimeter of a section through a CR-labeled dendrite was 2.95 μm. However, PV-labeled dendrites had an average of 0.2 asymmetric synapses per micron and an average of 0.02 symmetric synapses per micron, whereas CR-labeled dendrites had an average of 0.1 asymmetric synapses per micron and an average of 0.05 symmetric synapses per micron. The differences in frequency and density of synaptic inputs on PV- and CR-labeled dendrites can be seen in Figures 6 and 10–12.

D1R-IR in Terminals Contacting PV and CR Dendrites

D1R have been identified on axon terminals in the current and previous studies (Muly et al. 1998; Paspalas and Goldman-Rakic 2005; Bordelon-Glausier et al. 2008). Electrophysiological studies indicate that D1R ligands can have presynaptic effects on pyramidal cell–fast spiking cell pairs (Gonzalez-Burgos, Krimer, et al. 2005) and fast spiking–fast spiking interneuron pairs (Towers and Hestrin 2008). Therefore, we analyzed the prevalence of D1R-IR on axon terminals contacting PV- and CR-labeled dendrites. In material double labeled for D_1 and PV, only 1.2% (2 of 165) of terminals synapsing onto PV-labeled dendrites contained label for D_1. One D_1-IR axon terminal made an asymmetric synapse, whereas the other was symmetric. In material double labeled for D_5 and PV, 4.1% (6 of 147) of terminals synapsing onto PV-labeled dendrites contained label for D_5, and each of these synapses was asymmetric. In material double labeled for D_1 and CR, none of the terminals synapsing onto CR-labeled dendrites contained label for D_1 (0 of 81). Finally, in material double labeled for D_5 and CR, 3.1% (4 of 128) of terminals synapsing onto CR-labeled dendrites contained label for D_5. Two of the synapses were asymmetric, and the remaining 2 were symmetric. These results suggest that the axon terminals that synapse onto inhibitory interneurons contain D1R at a relatively low frequency. D_5-IR appears to be found more frequently in these axon terminals; however,

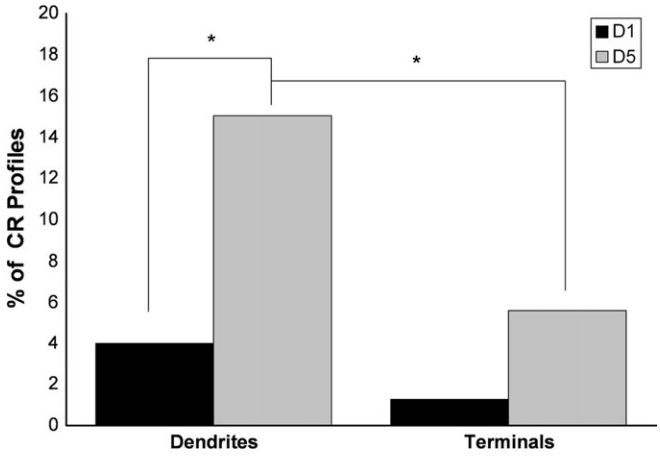

Figure 8. A histogram showing the percentage of CR-labeled dendrites and axon terminals that also contained IR for D_1 and D_5. In the D_1/CR condition, 276 dendrites and 79 axon terminals in total were counted. In the D_5/CR condition, 313 dendrites and 139 axon terminals in total were counted. The frequency of D_5/CR dendrites (15.0%) is greater than the frequency of D_1/CR dendrites (4.0%). The number of CR-IR axon terminals in the D_1 double-label condition was not sufficient to permit a valid statistical analysis between D_1/CR and D_5/CR. The D_5 receptor is more prevalent in CR dendrites (14.8%) than in CR axon terminals (5.8%). Asterisks indicate a significant difference.

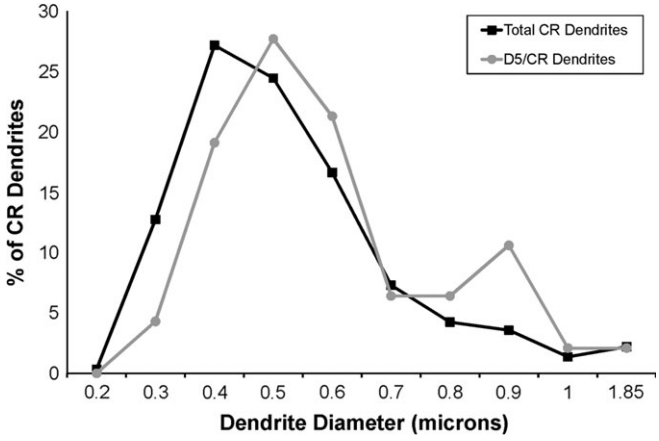

Figure 9. Graph illustrating the distribution of all CR dendritic diameters ($N = 589$) and the distribution of the diameters of D_5/CR double-labeled dendrites ($N = 47$). The majority of CR dendrites had diameters between 0.4 and 0.5 μm in diameter, and the majority of D_5/CR double-labeled dendrites had diameters between 0.4 and 0.6 μm. These results indicate that D_5-IR is not found preferentially in small (distal) or large (proximal) caliber CR dendrites.

the numbers of labeled terminals in each condition are too low to make a valid statistical comparison at this time.

Discussion

In the present study, we determined the subcellular localization of the D_1 and D_5 dopamine receptors in 2 different classes of interneurons defined by their content of PV or CR within layer III of prefrontal cortical area 9 in *M. mulatta* monkeys. The D_1 receptor is the major D1R subtype in PV interneurons where it is present in approximately 17% of PV dendritic profiles. D_5 is the predominant D1R subtype in CR interneurons, where it is present in approximately 15% of CR dendritic profiles. PV dendrites were also found to receive twice the density of asymmetric synapses than CR dendrites, and D1R-IR was identified on axon terminals contacting PV- and CR-labeled dendrites. Though their total number was relatively small, the data suggest that there could be a limited presynaptic D1R effect for inputs to PV and CR interneurons or that the effect is limited to a subset of these interneurons.

A previous immunofluorescence study examining D_1-IR in the cell bodies of PV and CR interneurons determined that 98% of PV interneurons contained D_1, whereas approximately 40% of CR interneurons contained D_1 (Muly et al. 1998). Consistent with these previous results, we identified the D_1 receptor more frequently in PV dendrites and axon terminals than in CR components. At first glance, the degree of colocalization in these 2 studies appears different; however, in the current study, we examined single, ultrathin sections (ca. 60 nm thick), thus only observing a very small region of any particular dendrite. This coupled with the patchy nature of D1R-IR suggests that even if every single PV dendrite contained D_1 receptor, not every ultrathin section of a PV dendrite might be double labeled. The patchiness of the D1R-IR has allowed us to make some observations on the localization of D_1 and D_5 within labeled dendrites. Our analysis of single sections found that roughly one-third of double-labeled dendrites exhibited DAB patches associated with the plasma membrane. Serial section analysis through PV and CR dendrites confirmed that although many patches of D1R-IR are located intracellularly, there is evidence for D1R-IR associated with the plasma membrane and even with synapses onto dendrites. Thus, the D1R are positioned to influence activity at the plasma membrane.

Our analysis of the dendritic diameter of single- and double-labeled interneuron dendrites did not find any evidence that D1R are biased to proximal or distal dendritic segments. There is evidence that interneuron dendrites taper with increased distance from the cell body, though the relationship is not as pronounced as it is in pyramidal cells (Jones 1975). Dendrites protruding from the cell body of some layer III interneurons can measure up to 10 μm in diameter and second order branching diameters of up to 5 μm have been reported (Jones 1975); however, we did not identify any PV or CR dendrites that large. The vast majority of PV and CR dendrites we identified and examined were less than 1 μm and between 0.4 and 0.6 μm in diameter, suggesting that our sample was mostly from dendrites at an intermediate distance from the cell body. Moreover, the distribution of double-labeled PV and CR dendrites mirrored the distribution of all PV and CR dendrites, demonstrating that there was not any preferential D1R labeling of large or small caliber dendrites.

Role of D1R Subtypes in Prefrontal Inhibitory Circuitry

Interneurons are a diverse group of cells, displaying various morphologies, electrophysiological properties, and synaptology (see reviews DeFelipe 1997; Markram et al. 2004). Importantly, PV and CR interneurons have very different postsynaptic targets. PV interneurons primarily synapse onto cell bodies, initial axon segments, and the proximal dendritic shafts of pyramidal cells (DeFelipe et al. 1989; Lewis and Lund 1990; Williams et al. 1992; Kawaguchi 1995), and activation of PV interneurons prevents action potentials in the pyramidal cells they innervate. On the other hand, CR interneurons primarily synapse onto other interneurons, including those containing PV (Gabbott and Bacon 1996; Gulyas et al. 1996; Meskenaite

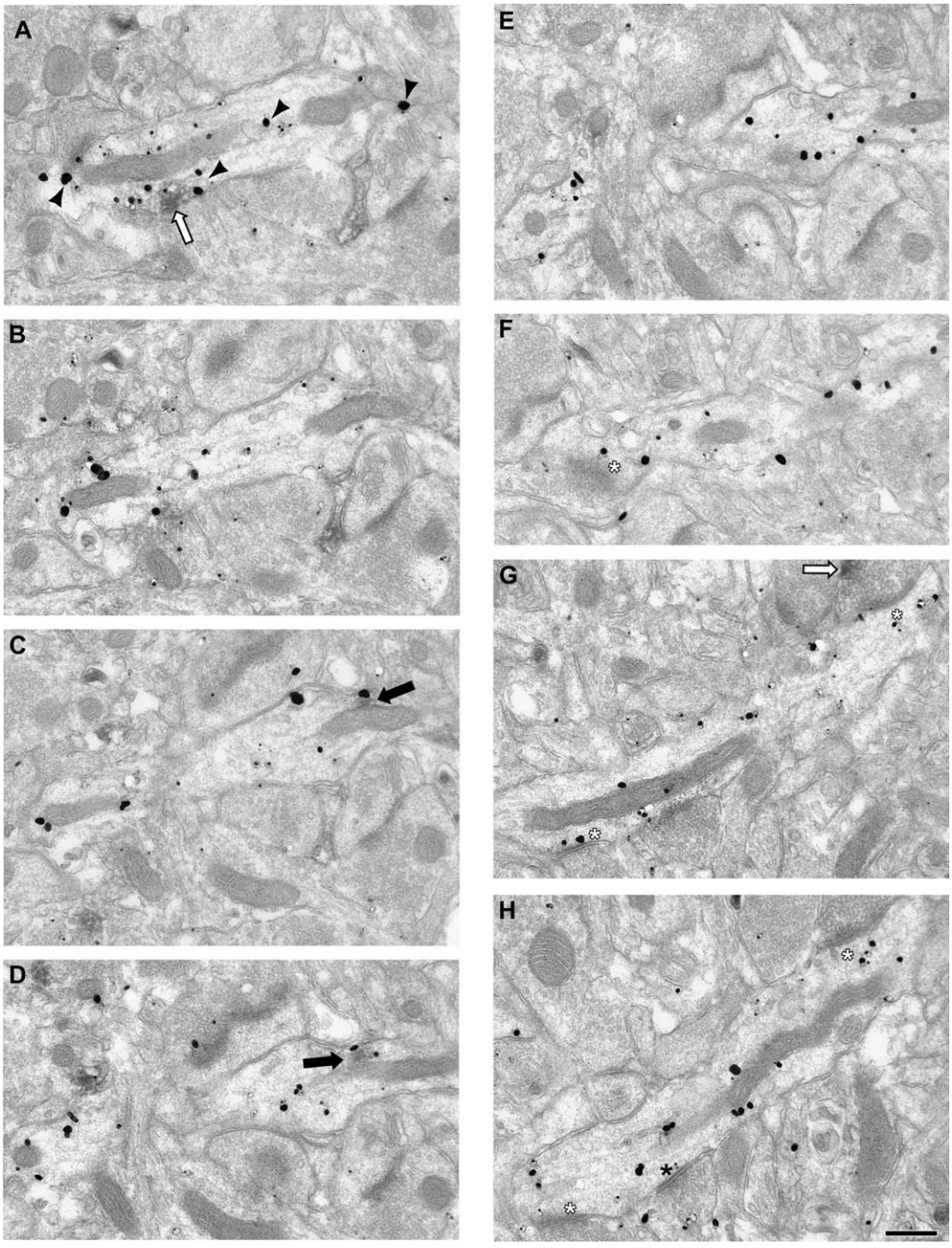

Figure 10. Electron micrographs illustrating the distribution of D_5-IR in serial sections of a CR-labeled dendrite. CR immunogold label is present throughout the dendrite and is identified by black arrowheads in panel (*A*). Patches of D_5-IR have been identified as intracellular (black arrow) or associated with the plasma membrane (white arrow). In panel (*A*), the D_5-IR is present and associated with the plasma membrane, whereas in panels (*C*, *D*), it is intracellular and associate with a mitochondria. No synapses are visible until panel (*F*), where an asymmetric synapse (white asterisk) is cut tangentially. In panels (*G–H*), the CR dendrite receives 2 asymmetric synapses and 1 symmetric (black asterisk). One terminal forming an asymmetric synapse contains D_5-IR (black arrow) visible in panel (*G*). Scale bar is 500 nm.

1997). Although data presented here and elsewhere indicate that most synapses onto PV interneurons are asymmetric and likely excitatory, PV interneurons do receive symmetric (presumably inhibitory) inputs (Williams et al. 1992). Inhibitory inputs onto PV interneurons are effective, producing faster, higher amplitude, and more frequent inhibitory postsynaptic potential (IPSP) than observed in other types of interneurons (Bacci et al. 2003). Taken together, these data indicate that PV and CR interneurons have discrete roles in controlling pyramidal cell output: PV cells strongly inhibit pyramidal cells, and CR cells disinhibit them by inhibiting other interneurons.

Inhibitory neurotransmission plays a powerful role in prefrontal function both at the behavioral and cellular level. Activation or inhibition of GABAergic signaling can impair WM performance, and blockade of inhibitory neurotransmission abolishes pyramidal delay cell activity (Sawaguchi et al. 1988, 1989; Rao et al. 2000; Sawaguchi and Iba 2001). Furthermore, inhibitory interneurons have been shown to display tuned

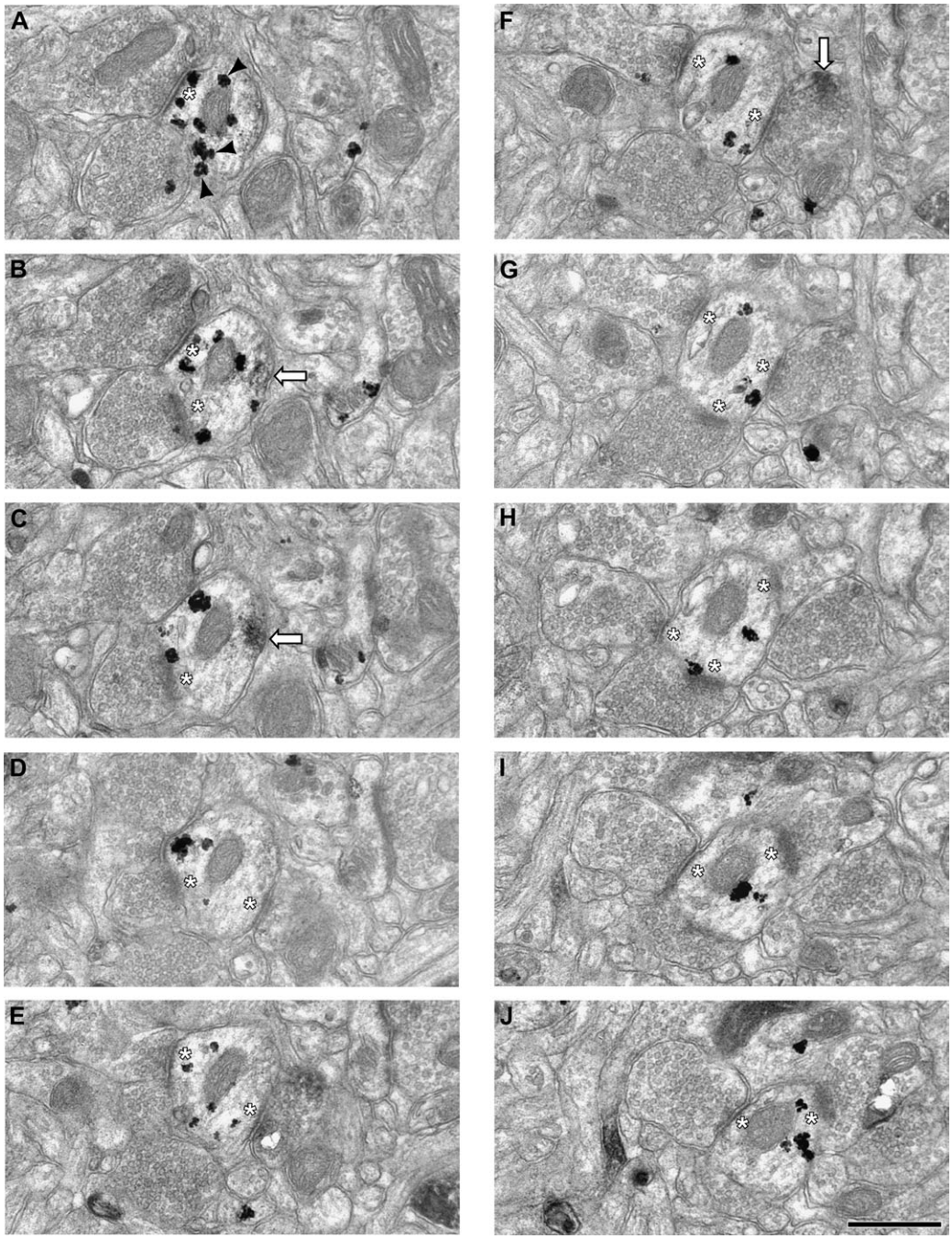

Figure 11. Electron micrographs illustrating the density of asymmetric synapses onto a PV-labeled dendrite which also contains D_1-IR. PV immunogold is present throughout the serial sections of this dendrite and is indicated by black arrowheads in panel (*A*). D_1-IR associated with the plasma membrane is present in panels (*B* and *C*) (white arrows). Over a total perimeter length of 19.8 μm, this PV-labeled dendrite received 7 asymmetric synapses (white asterisks) and has a density of 0.35 asymmetric synapses per micron of dendritic perimeter. One of the axon terminals making a synaptic contact onto this PV-labeled dendrite also contains D_1-IR associated with the plasma membrane (white arrow, panel *F*).

delay activity similar to pyramidal delay cells (Rao et al. 1999), and it has been proposed that they contribute to the specificity of pyramidal delay cells (Rao et al. 1999; Gonzalez-Burgos, Kroener, et al. 2005). Moreover, previous studies have demonstrated an interaction between D1R stimulation and GABAergic signaling, such that D1R activation generally excites interneurons by augmenting glutamate currents and various ionic currents (reviewed in Yang et al. 1999; Seamans and Yang 2004).

Differential receptor expression across interneuron subtypes has been reported previously (Vissavajjhala et al. 1996; Jakab and Goldman-Rakic 2000; Nyiri et al. 2003; Somogyi et al. 2003; Deng et al. 2007), and receptor heterogeneity could contribute to the varied electrophysiological responses seen in interneurons (Geiger et al. 1995; Bacci et al. 2003; Goldberg et al. 2003). Moreover, there is growing evidence for functional differences between D_1 and D_5. For example, D_1 interacts with the N-methyl-D-aspartic acid (NMDA) receptor (Lee et al.

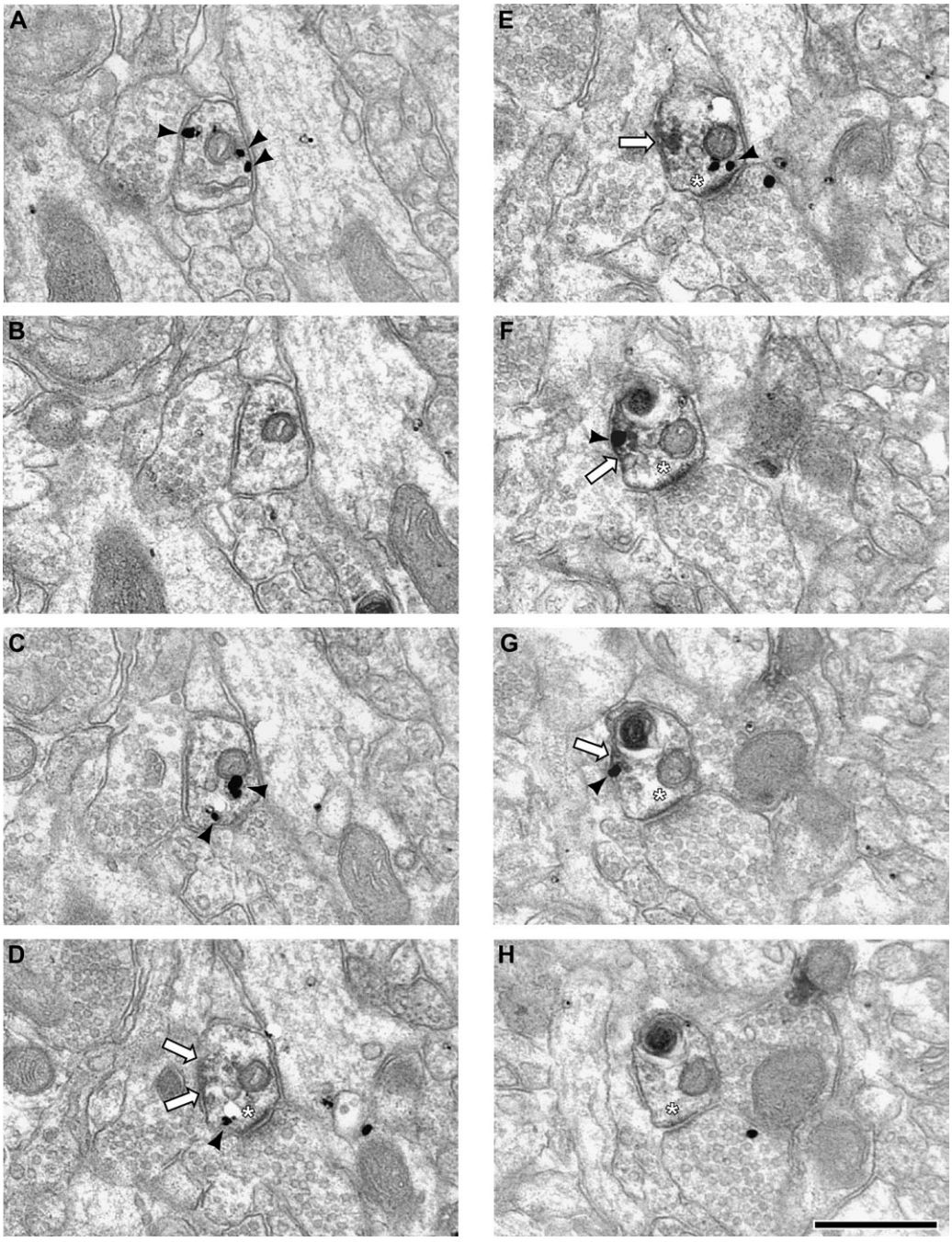

Figure 12. Electron micrographs illustrating the density of asymmetric synapses onto a CR-labeled dendrite which also contains D_5-IR. CR immunogold label is identified by black arrowheads and is labeled throughout the dendrite. Patches of D_5-IR have been identified as associated with the plasma membrane (white arrows). D_5-IR begins to appear in panel (*D*), where it is associated with the plasma membrane, and remains visible until panel (*G*). Over a total perimeter length of 10.2 μm, this CR-labeled dendrite received 1 asymmetric contact (white asterisk) and has a density of 0.1 asymmetric synapses per micron of dendritic perimeter. Scale bar is 500 nm.

2002), whereas D_5 interacts with the $GABA_A$ receptor (Liu et al. 2000); genetic deletion of D_1 impairs corticostriatal long-term potentiation (LTP), while blocking the remaining D_5 receptors impairs corticostriatal long-term depression (LTD) (Centonze et al. 2003); D_1 and D_5 have distinct effects on locomotion (Dziewczapolski et al. 1998; Centonze et al. 2003); and D_5 regulates acetylcholine release in the mouse hippocampus (Laplante et al. 2004) and has higher constitutive activity (Tiberi and Caron 1994). One difference that is particularly relevant for understanding the dose-dependent relationship between D1R stimulation and WM performance/delay cell tuning is the 10-fold higher affinity for dopamine exhibited by the D_5 receptor (Sunahara et al. 1991; Weinshank et al. 1991; Tiberi and Caron 1994). The preferential expression of D_1 in PV interneurons and D_5 in CR interneurons suggests that as the concentration of dopamine in the PFC changes, different populations of interneurons would be modulated via D1R stimulation.

The inverted-U relationship between D1R activity and WM performance/delay cell tuning is well documented (reviewed

in Williams and Castner 2006). Peak delay cell firing rates are seen with low levels of D1R stimulation (Vijayraghavan et al. 2007). Delay cell activity decreases both as D1R stimulation increases (Williams and Goldman-Rakic 1995; Vijayraghavan et al. 2007) and when D1R is completely blocked by high ejection current application of specific antagonists (Williams and Goldman-Rakic 1995; Sawaguchi 2001). Interestingly, Vijayraghavan et al. (2007) have demonstrated that the optimal signal to noise ratio of delay activity is not associated with maximal cell firing rate but rather is observed at higher levels of D1R stimulation when overall firing rates are moderate (see their Fig. 1*B*). These observed relationships between D1R stimulation and cell activity and delay signal to noise levels are illustrated in Figure 13*A*.

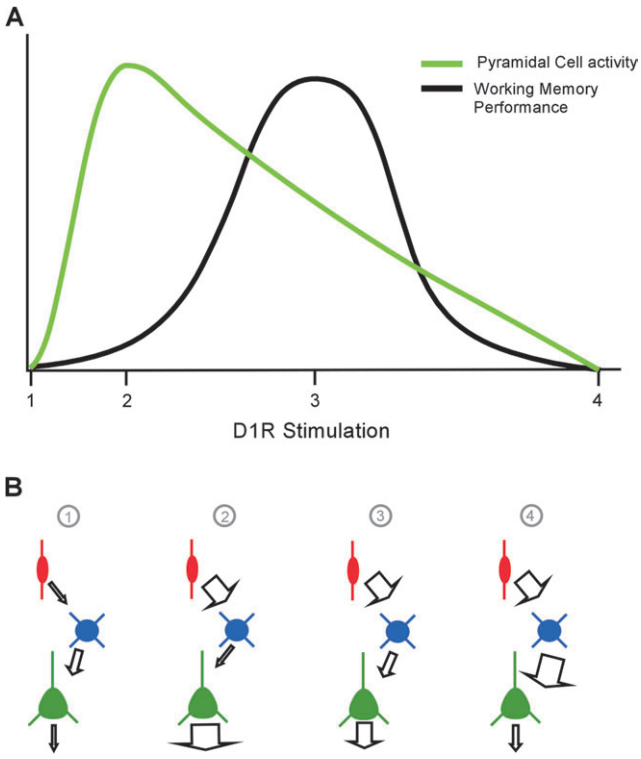

Figure 13. (*A*) Graphical representation of the relationship between D1R stimulation and pyramidal cell activity (green) or WM performance (black). Different levels of D1R stimulation are indicated by numbers on the *x*-axis. Point 1 represents no D1R stimulation, resulting in very little pyramidal cell output and poor WM performance. Point 2 represents low levels of D1R stimulation, with strong pyramidal cell activity but with suboptimal WM performance. Point 3 represents moderate levels of D1R stimulation. At this point, pyramidal cell activity is lower, but WM performance is optimal. Finally, point 4 represents high levels of D1R stimulation, and both pyramidal cell activity and WM performance are diminished. Note that although both pyramidal cell activity and WM performance have inverted-U relationships with D1R activation, the cell activity peak is left shifted compared with WM performance. (*B*) Simplified circuit model of the relationship between CR interneurons (red), PV interneurons (blue), and pyramidal cells (green). Panel 1 represents activity levels with there is no D1R stimulation. Panel 2 represents cellular activity levels at low D1R stimulation. D_5 receptors on CR interneurons would be preferentially activated, enhancing their output, resulting in decreased PV interneuron activity, and disinhibiting the pyramidal cell. Panel 3 represents cellular activity levels at moderate D1R stimulation. Whereas D_5 receptors on CR interneurons are still being activated, D_1 receptors on PV interneurons are also now stimulated, allowing the PV interneurons to overcome some of the inhibition by CR interneurons which in turn results in decreased pyramidal cell activity. Finally, panel 4 represents cellular activity levels at high D1R stimulation. D_1 receptors on the PV interneurons are now maximally stimulated, overriding most of the inhibition from CR interneurons. PV interneuron activity will be greatly enhanced, resulting in a dramatic reduction in pyramidal cell output.

The data presented here on differential localization of D_1 and D_5 to PV and CR interneurons, respectively, along with the known connectivity of these cell types and differential receptor affinities for dopamine suggest a circuit mechanism by which D1R stimulation can control pyramidal cell output (Fig. 13*B*). Panel 1 reflects the output when there is no D1R stimulation, a condition which might only be induced experimentally with high doses of D1R antagonist or dopamine depletion and in which there is no D1R-mediated augmentation of glutamate currents. Panel 2 reflects the activity of these cells when there are low levels of dopamine. The D_5 receptors found on CR interneurons and pyramidal cell spines (Bordelon-Glausier et al. 2008) are preferentially activated due to their higher affinity for dopamine. Activation of G_s-coupled D_5 would be expected to augment glutamatergic inputs to these pyramidal cell spines as well as to CR interneurons (reviewed in Seamans and Yang 2004). The increased activation of CR interneurons would increase inhibition of their postsynaptic targets, including PV interneurons, resulting in disinhibition and peak activity levels of their pyramidal cell targets. As dopamine levels rise, the activation of D_5 receptors would eventually plateau, whereas D_1 receptors on PV interneurons and pyramidal cell spines would begin to be activated. Glutamatergic neurotransmission in these circuitry components will be increasingly augmented, eventually allowing PV interneurons to escape from the inhibitory control of CR cell. As PV interneuron activity increases, pyramidal cell output would decrease accordingly (Fig. 13; panels 3 and 4) but not completely because D_1 and D_5 on pyramidal cell spines would be concurrently activated.

The model proposed here provides a circuit basis for understanding the relationship between dopamine stimulation of D1R and overall activity of pyramidal delay neurons. However, additional work will be required to resolve several issues. First, this model does not consider data indicating that the PV interneurons receive more direct dopaminergic input than CR interneurons (Sesack, Bressler, and Lewis 1995; Krimer et al. 1997; Sesack et al. 1998). Whereas this may impact the access these interneurons have to dopamine, in the PFC, D1R are not seen at symmetric synapses (Smiley et al. 1994; Muly et al. 1998; Bordelon-Glausier et al. 2008), the morphology of dopaminergic synapses (Goldman-Rakic et al. 1989; Sesack, Synder, and Lewis 1995). Thus, extrasynaptic transmission is the primary means of D1R activation in the PFC. Second, this model cannot explain existing in vivo studies show that D1R stimulation produces a preferential decrease in activity for the nonpreferred direction in spatially tuned delay cells (Sawaguchi 2001; Vijayraghavan et al. 2007). The mechanism by which this is achieved is unclear, though it may relate to the wider tangential spread of the axons and dendrites of PV compared with CR interneurons (reviewed in DeFelipe 1997), allowing pyramidal cells to be inhibited by PV interneurons from adjacent columns of cortex with slightly different response properties. It is also possible that different classes of interneurons contain different sets of signal transduction proteins, as has been shown for pyramidal cell spines (Muly et al. 2001), and that activation of a D1R might effect CR interneurons differently than PV interneurons. A detailed knowledge of the signaling environments, as well as the

localization of D1R on other interneuron classes of the PFC, may provide further insight into the inverted-U relationship between D1R stimulation and WM performance.

Funding

National Institutes of Health (MH076372 to J.R.G., MH068789 to E.C.M., RR00165); the Department of Veterans Affairs (Merit Award to E.C.M); and the Ministerio de Educacíon y Ciencia (BFU 2006-00306 to Z.U.K).

Notes

The authors gratefully acknowledge the excellent technical assistance of Marcelia Maddox and thank Dr Yoland Smith for his critical reading of the manuscript. *Conflict of Interest*: None declared.

Address correspondence to email: emuly@emory.edu.

References

Bacci A, Rudolph U, Huguenard JR, Prince DA. 2003. Major differences in inhibitory synaptic transmission onto two neocortical interneuron subclasses. J Neurosci. 23:9664–9674.

Bordelon-Glausier JR, Khan ZU, Muly EC. 2008. Quantification of D1 and D5 dopamine receptor localization in layers I, III, and V of *Macaca mulatta* prefrontal cortical area 9: coexpression in dendritic spines and axon terminals. J Comp Neurol. 508:893–905.

Brozoski TJ, Brown RM, Rosvold HE, Goldman PS. 1979. Cognitive deficit caused by regional depletion of dopamine in prefrontal cortex of rhesus monkey. Science. 205:929–932.

Celio MR. 1986. Parvalbumin in most gamma-aminobutyric acid-containing neurons of the rat cerebral cortex. Science. 231: 995–997.

Centonze D, Grande C, Saulle E, Martin AB, Gubellini P, Pavon N, Pisani A, Bernardi G, Moratalla R, Calabresi P. 2003. Distinct roles of D1 and D5 dopamine receptors in motor activity and striatal synaptic plasticity. J Neurosci. 23:8506–8512.

Conde F, Lund JS, Jacobowitz DM, Baimbridge KG, Lewis DA. 1994. Local circuit neurons immunoreactive for calretinin, calbindin D-28k or parvalbumin in monkey prefrontal cortex: distribution and morphology. J Comp Neurol. 341:95–116.

DeFelipe J. 1997. Types of neurons, synaptic connections and chemical characteristics of cells immunoreactive for calbindin-D28K, parvalbumin and calretinin in the neocortex. J Chem Neuroanat. 14:1–19.

DeFelipe J, Hendry SH, Jones EG. 1989. Visualization of chandelier cell axons by parvalbumin immunoreactivity in monkey cerebral cortex. Proc Natl Acad Sci USA. 86:2093–2097.

Deng YP, Xie JP, Wang HB, Lei WL, Chen Q, Reiner A. 2007. Differential localization of the GluR1 and GluR2 subunits of the AMPA-type glutamate receptor among striatal neuron types in rats. J Chem Neuroanat. 33:167–192.

Disney AA, Domakonda KV, Aoki C. 2006. Differential expression of muscarinic acetylcholine receptors across excitatory and inhibitory cells in visual cortical areas V1 and V2 of the macaque monkey. J Comp Neurol. 499:49–63.

Dziewczapolski G, Menalled LB, Garcia MC, Mora MA, Gershanik OS, Rubinstein M. 1998. Opposite roles of D1 and D5 dopamine receptors in locomotion revealed by selective antisense oligonucleotides. Neuroreport. 9:1–5.

Gabbott PL, Bacon SJ. 1996. Local circuit neurons in the medial prefrontal cortex (areas 24a,b,c, 25 and 32) in the monkey: I. Cell morphology and morphometrics. J Comp Neurol. 364:567–608.

Geiger JR, Melcher T, Koh DS, Sakmann B, Seeburg PH, Jonas P, Monyer H. 1995. Relative abundance of subunit mRNAs determines gating and Ca2+ permeability of AMPA receptors in principal neurons and interneurons in rat CNS. Neuron. 15:193–204.

Giguere M, Goldman-Rakic PS. 1988. Mediodorsal nucleus: areal, laminar, and tangential distribution of afferents and efferents in the frontal lobe of rhesus monkeys. J Comp Neurol. 277:195–213.

Goldberg JH, Yuste R, Tamas G. 2003. Ca2+ imaging of mouse neocortical interneurone dendrites: contribution of Ca2+-permeable AMPA and NMDA receptors to subthreshold Ca2+dynamics. J Physiol. 551:67–78.

Goldman-Rakic PS, Leranth C, Williams SM, Mons N, Geffard M. 1989. Dopamine synaptic complex with pyramidal neurons in primate cerebral cortex. Proc Natl Acad Sci USA. 86:9015–9019.

Goldman-Rakic PS, Muly EC, 3rd, Williams GV. 2000. D(1) receptors in prefrontal cells and circuits. Brain Res Brain Res Rev. 31: 295–301.

Goldman-Rakic PS, Porrino LJ. 1985. The primate mediodorsal (MD) nucleus and its projection to the frontal lobe. J Comp Neurol. 242:535–560.

Gonchar Y, Burkhalter A. 1997. Three distinct families of GABAergic neurons in rat visual cortex. Cereb Cortex. 7:347–358.

Gonzalez-Burgos G, Krimer LS, Povysheva NV, Barrionuevo G, Lewis DA. 2005. Functional properties of fast spiking interneurons and their synaptic connections with pyramidal cells in primate dorsolateral prefrontal cortex. J Neurophysiol. 93:942–953.

Gonzalez-Burgos G, Kroener S, Seamans JK, Lewis DA, Barrionuevo G. 2005. Dopaminergic modulation of short-term synaptic plasticity in fast-spiking interneurons of primate dorsolateral prefrontal cortex. J Neurophysiol. 94:4168–4177.

Grandy DK, Zhang YA, Bouvier C, Zhou QY, Johnson RA, Allen L, Buck K, Bunzow JR, Salon J, Civelli O. 1991. Multiple human D5 dopamine receptor genes: a functional receptor and two pseudogenes. Proc Natl Acad Sci USA. 88:9175–9179.

Gulyas AI, Hajos N, Freund TF. 1996. Interneurons containing calretinin are specialized to control other interneurons in the rat hippocampus. J Neurosci. 16:3397–3411.

Heizmann CW, Celio MR. 1987. Immunolocalization of parvalbumin. Methods Enzymol. 139:552–570.

Hersch SM, Ciliax BJ, Gutekunst CA, Rees HD, Heilman CJ, Yung KK, Bolam JP, Ince E, Yi H, Levey AI. 1995. Electron microscopic analysis of D1 and D2 dopamine receptor proteins in the dorsal striatum and their synaptic relationships with motor corticostriatal afferents. J Neurosci. 15:5222–5237.

Jakab RL, Goldman-Rakic PS. 2000. Segregation of serotonin 5-HT2A and 5-HT3 receptors in inhibitory circuits of the primate cerebral cortex. J Comp Neurol. 417:337–348.

Jones EG. 1975. Varieties and distribution of non-pyramidal cells in the somatic sensory cortex of the squirrel monkey. J Comp Neurol. 160:205–267.

Jones EG, Hendry SH. 1989. Differential calcium binding protein immunoreactivity distinguishes classes of relay neurons in monkey thalamic nuclei. Eur J Neurosci. 1:222–246.

Kawaguchi Y. 1995. Physiological subgroups of nonpyramidal cells with specific morphological characteristics in layer II/III of rat frontal cortex. J Neurosci. 15:2638–2655.

Kawaguchi Y, Kubota Y. 1997. GABAergic cell subtypes and their synaptic connections in rat frontal cortex. Cereb Cortex. 7:476–486.

Khan ZU, Gutierrez A, Martin R, Penafiel A, Rivera A, de la Calle A. 2000. Dopamine D5 receptors of rat and human brain. Neuroscience. 100:689–699.

Krimer LS, Jakab RL, Goldman-Rakic PS. 1997. Quantitative three-dimensional analysis of the catecholaminergic innervation of identified neurons in the macaque prefrontal cortex. J Neurosci. 17:7450–7461.

Kritzer MF, Goldman-Rakic PS. 1995. Intrinsic circuit organization of the major layers and sublayers of the dorsolateral prefrontal cortex in the rhesus monkey. J Comp Neurol. 359:131–143.

Laplante F, Sibley DR, Quirion R. 2004. Reduction in acetylcholine release in the hippocampus of dopamine D5 receptor-deficient mice. Neuropsychopharmacology. 29:1620–1627.

Lee FJ, Xue S, Pei L, Vukusic B, Chery N, Wang Y, Wang YT, Niznik HB, Yu XM, Liu F. 2002. Dual regulation of NMDA receptor functions by direct protein-protein interactions with the dopamine D1 receptor. Cell. 111:219–230.

Lewis DA, Lund JS. 1990. Heterogeneity of chandelier neurons in monkey neocortex: corticotropin-releasing factor- and parvalbumin-immunoreactive populations. J Comp Neurol. 293:599–615.

Liu F, Wan Q, Pristupa ZB, Yu XM, Wang YT, Niznik HB. 2000. Direct protein-protein coupling enables cross-talk between dopamine D5 and GABA A receptors. Nature. 403:274–280.

Lund JS, Lewis DA. 1993. Local circuit neurons of developing and mature macaque prefrontal cortex: golgi and immunocytochemical characteristics. J Comp Neurol. 328:282–312.

Markram H, Toledo-Rodriguez M, Wang Y, Gupta A, Silberberg G, Wu C. 2004. Interneurons of the neocortical inhibitory system. Nat Rev Neurosci. 5:793–807.

Maunsell JH, van Essen DC. 1983. The connections of the middle temporal visual area (MT) and their relationship to a cortical hierarchy in the macaque monkey. J Neurosci. 3:2563–2586.

Melchitzky DS, Eggan SM, Lewis DA. 2005. Synaptic targets of calretinin-containing axon terminals in macaque monkey prefrontal cortex. Neuroscience. 130:185–195.

Melchitzky DS, Lewis DA. 2003. Pyramidal neuron local axon terminals in monkey prefrontal cortex: differential targeting of subclasses of GABA neurons. Cereb Cortex. 13:452–460.

Melchitzky DS, Lewis DA. 2008. Dendritic-targeting GABA neurons in monkey prefrontal cortex: comparison of somatostatin- and calretinin-immunoreactive axon terminals. Synapse. 62:456–465.

Melchitzky DS, Sesack SR, Lewis DA. 1999. Parvalbumin-immunoreactive axon terminals in macaque monkey and human prefrontal cortex: laminar, regional, and target specificity of type I and type II synapses. J Comp Neurol. 408:11–22.

Meskenaite V. 1997. Calretinin-immunoreactive local circuit neurons in area 17 of the cynomolgus monkey, *Macaca fascicularis*. J Comp Neurol. 379:113–132.

Muller U, von Cramon DY, Pollmann S. 1998. D1- versus D2-receptor modulation of visuospatial working memory in humans. J Neurosci. 18:2720–2728.

Muly EC, Greengard P, Goldman-Rakic PS. 2001. Distribution of protein phosphatases-1 alpha and -1 gamma 1 and the D(1) dopamine receptor in primate prefrontal cortex: evidence for discrete populations of spines. J Comp Neurol. 440:261–270.

Muly EC, Szigeti K, Goldman-Rakic PS. 1998. D1 receptor in interneurons of macaque prefrontal cortex: distribution and subcellular localization. J Neurosci. 18:10553–10565.

Nyiri G, Stephenson FA, Freund TF, Somogyi P. 2003. Large variability in synaptic N-methyl-D-aspartate receptor density on interneurons and a comparison with pyramidal-cell spines in the rat hippocampus. Neuroscience. 119:347–363.

Park HS, Park SJ, Park SH, Chun MH, Oh SJ. 2008. Shifting of parvalbumin expression in the rat retina in experimentally induced diabetes. Acta Neuropathol. 115:241–248.

Paspalas CD, Goldman-Rakic PS. 2005. Presynaptic D1 dopamine receptors in primate prefrontal cortex: target-specific expression in the glutamatergic synapse. J Neurosci. 25:1260–1267.

Peters A. 1987. Synaptic specificity in the cerebral cortex. In: Edelman GM, Gall WE, Cowan WM, editors. Syanptic function. New York: John Wiley and Sons. p. 373–397.

Peters A, Jones EG, (editors). 1984. Cerebral cortex. New York: Plenum Press.

Rao SG, Williams GV, Goldman-Rakic PS. 1999. Isodirectional tuning of adjacent interneurons and pyramidal cells during working memory: evidence for microcolumnar organization in PFC. J Neurophysiol. 81:1903–1916.

Rao SG, Williams GV, Goldman-Rakic PS. 2000. Destruction and creation of spatial tuning by disinhibition: GABA(A) blockade of prefrontal cortical neurons engaged by working memory. J Neurosci. 20:485–494.

Rockland KS, Pandya DN. 1979. Laminar origins and terminations of cortical connections of the occipital lobe in the rhesus monkey. Brain Res. 179:3–20.

Sarro EC, Kotak VC, Sanes DH, Aoki C. Hearing loss alters the subcellular distribution of presynaptic GAD and postsynaptic GABA(A) receptors in the auditory cortex. Cereb Cortex. Advance Access published April 9, 2008, doi:10.1093/cercor/bhn044.

Sawaguchi T. 2001. The effects of dopamine and its antagonists on directional delay-period activity of prefrontal neurons in monkeys during an oculomotor delayed-response task. Neurosci Res. 41:115–128.

Sawaguchi T, Goldman-Rakic PS. 1991. D1 dopamine receptors in prefrontal cortex: involvement in working memory. Science. 251:947–950.

Sawaguchi T, Iba M. 2001. Prefrontal cortical representation of visuospatial working memory in monkeys examined by local inactivation with muscimol. J Neurophysiol. 86:2041–2053.

Sawaguchi T, Matsumura M, Kubota K. 1988. Delayed response deficit in monkeys by locally disturbed prefrontal neuronal activity by bicuculline. Behav Brain Res. 31:193–198.

Sawaguchi T, Matsumura M, Kubota K. 1989. Delayed response deficits produced by local injection of bicuculline into the dorsolateral prefrontal cortex in Japanese macaque monkeys. Exp Brain Res. 75:457–469.

Seamans JK, Yang CR. 2004. The principal features and mechanisms of dopamine modulation in the prefrontal cortex. Prog Neurobiol. 74:1–58.

Sesack SR, Bressler CN, Lewis DA. 1995. Ultrastructural associations between dopamine terminals and local circuit neurons in the monkey prefrontal cortex: a study of calretinin-immunoreactive cells. Neurosci Lett. 200:9–12.

Sesack SR, Hawrylak VA, Melchitzky DS, Lewis DA. 1998. Dopamine innervation of a subclass of local circuit neurons in monkey prefrontal cortex: ultrastructural analysis of tyrosine hydroxylase and parvalbumin immunoreactive structures. Cereb Cortex. 8:614–622.

Sesack SR, Snyder CL, Lewis DA. 1995. Axon terminals immunolabeled for dopamine or tyrosine hydroxylase synapse on GABA-immunoreactive dendrites in rat and monkey cortex. J Comp Neurol. 363:264–280.

Smiley JF, Levey AI, Ciliax BJ, Goldman-Rakic PS. 1994. D1 dopamine receptor immunoreactivity in human and monkey cerebral cortex: predominant and extrasynaptic localization in dendritic spines. Proc Natl Acad Sci USA. 91:5720–5724.

Somogyi P, Dalezios Y, Lujan R, Roberts JD, Watanabe M, Shigemoto R. 2003. High level of mGluR7 in the presynaptic active zones of select populations of GABAergic terminals innervating interneurons in the rat hippocampus. Eur J Neurosci. 17:2503–2520.

Sunahara RK, Guan HC, O'Dowd BF, Seeman P, Laurier LG, Ng G, George SR, Torchia J, Van Tol HH, Niznik HB. 1991. Cloning of the gene for a human dopamine D5 receptor with higher affinity for dopamine than D1. Nature. 350:614–619.

Tiberi M, Caron MG. 1994. High agonist-independent activity is a distinguishing feature of the dopamine D1B receptor subtype. J Biol Chem. 269:27925–27931.

Tiberi M, Jarvie KR, Silvia C, Falardeau P, Gingrich JA, Godinot N, Bertrand L, Yang-Feng TL, Fremeau RT Jr., Caron MG. 1991. Cloning, molecular characterization, and chromosomal assignment of a gene encoding a second D1 dopamine receptor subtype: differential expression pattern in rat brain compared with the D1A receptor. Proc Natl Acad Sci USA. 88:7491–7495.

Towers SK, Hestrin S. 2008. D1-like dopamine receptor activation modulates GABAergic inhibition but not electrical coupling between neocortical fast-spiking interneurons. J Neurosci. 28: 2633–2641.

Vijayraghavan S, Wang M, Birnbaum SG, Williams GV, Arnsten AF. 2007. Inverted-U dopamine D1 receptor actions on prefrontal neurons engaged in working memory. Nat Neurosci. 10:376–384.

Vissavajjhala P, Janssen WG, Hu Y, Gazzaley AH, Moran T, Hof PR, Morrison JH. 1996. Synaptic distribution of the AMPA-GluR2 subunit and its colocalization with calcium-binding proteins in rat cerebral cortex: an immunohistochemical study using a GluR2-specific monoclonal antibody. Exp Neurol. 142:296–312.

Walker A. 1940. A cytoarchitectural study of the prefrontal area of the macaque monkey. J Comp Neurol. 73:59–86.

Wang XJ, Tegner J, Constantinidis C, Goldman-Rakic PS. 2004. Division of labor among distinct subtypes of inhibitory neurons in a cortical microcircuit of working memory. Proc Natl Acad Sci USA. 101:1368–1373.

Weinshank RL, Adham N, Macchi M, Olsen MA, Branchek TA, Hartig PR. 1991. Molecular cloning and characterization of a high affinity dopamine receptor (D1 beta) and its pseudogene. J Biol Chem. 266:22427–22435.

Williams GV, Castner SA. 2006. Under the curve: critical issues for elucidating D1 receptor function in working memory. Neuroscience. 139:263–276.
Williams GV, Goldman-Rakic PS. 1995. Modulation of memory fields by dopamine D1 receptors in prefrontal cortex. Nature. 376:572–575.
Williams SM, Goldman-Rakic PS, Leranth C. 1992. The synaptology of parvalbumin-immunoreactive neurons in the primate prefrontal cortex. J Comp Neurol. 320:353–369.
Wilson FA, O'Scalaidhe SP, Goldman-Rakic PS. 1994. Functional synergism between putative gamma-aminobutyrate-containing neurons and pyramidal neurons in prefrontal cortex. Proc Natl Acad Sci USA. 91:4009–4013.
Yang CR, Seamans JK, Gorelova N. 1999. Developing a neuronal model for the pathophysiology of schizophrenia based on the nature of electrophysiological actions of dopamine in the prefrontal cortex. Neuropsychopharmacology. 21:161–194.
Zimmermann L, Schwaller B. 2002. Monoclonal antibodies recognizing epitopes of calretinins: dependence on Ca2+-binding status and differences in antigen accessibility in colon cancer cells. Cell Calcium. 31:13–25.